BIOCHEMISTRY
including biophysical chemistry & molecular biology

Article

pubs.acs.org/biochemistry

Interconversion of Active and Inactive Conformations of Urokinase-Type Plasminogen Activator

Zhuo Liu,[‡,§] Tobias Kromann-Hansen,[‡,§] Ida K. Lund,[#,⊥] Masood Hosseini,[∥,‡] Knud J. Jensen,[∥,‡] Gunilla Høyer-Hansen,[#,⊥] Peter A. Andreasen,[‡,§] and Hans Peter Sørensen*[,‡,§]

[‡]Danish-Chinese Centre for Proteases and Cancer and [§]Department of Molecular Biology and Genetics, Aarhus University, Denmark

[#]The Finsen Laboratory, Copenhagen University Hospital, Denmark

[⊥]Biotech Research and Innovation Centre (BRIC), University of Copenhagen, Denmark

[∥]Department of Chemistry, Faculty of Science, University of Copenhagen, Denmark

Supporting Information

ABSTRACT: The catalytic activity of serine proteases depends on a salt-bridge between the amino group of residue 16 and the side chain of Asp194. The salt-bridge stabilizes the oxyanion hole and the S1 specificity pocket of the protease. Some serine proteases exist in only partially active forms, in which the amino group of residue 16 is exposed to the solvent. Such a partially active state is assumed by a truncated form of the murine urokinase-type plasminogen activator (muPA), consisting of residues 16−243. Here we investigated the allosteric interconversion between partially active states and the fully active state. Both a monoclonal antibody (mU3) and a peptidic inhibitor (mupain-1−16) stabilize the active state. The epitope of mU3 is located in the 37- and 70-loops at a site homologous to exosite I of thrombin. The N-terminus$^{(Ile16)}$ of muPA$^{(16-243)}$ was less exposed upon binding of mU3 or mupain-1−16. In contrast, introduction of the mutations F40Y or E137A into muPA$^{(16-243)}$ increased exposure of the N-terminus$^{(Ile16)}$ and resulted in large changes in the thermodynamic parameters for mupain-1−16 binding. We conclude that the distorted state of muPA$^{(16-243)}$ is conformationally ordered upon binding of ligands to the active site and upon binding of mU3 to the 37- and 70-loops. Our study establishes the 37- and 70-loops as a unique site for binding to compounds stabilizing the active state of serine proteases.

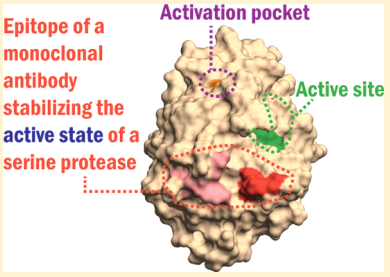

Trypsin-like serine proteases are synthesized inside the cell, secreted as inactive zymogens, and subsequently converted into active enzymes by proteolysis between residue 15 and 16[a].[1] The inactivity of serine protease zymogens results from improper formation of the S1 specificity pocket and the oxyanion hole.[2] The zymogen-activation domain, generally composed of residues 142−153, 184−194, and 215−225, shows an altered structure or conformational flexibility in crystal structures of zymogens relative to structures of active proteases. Proteolytic cleavage following residue 15 triggers the nascent N-terminus at position 16 to form a salt-bridge to Asp194, located at the bottom of the activation pocket. This salt-bridge stabilizes the oxyanion hole and the S1 specificity pocket. The activated catalytic domain formed by this transition exhibits a conformation, which changes depending on the binding of substrates and inhibitors to the active site or cofactors to exosites.[3] Thrombin, Factor VIIa, and complement factor D represent classical examples of serine proteases, which in the absence of substrates, inhibitors, or cofactors exhibit a resting low activity conformation, which seems to be more flexible than the active conformation.[4−7] Ligand-free thrombin rests in a catalytically inefficient state but assumes the fully active conformation upon binding of ligands to exosite I or inhibitors and substrates to the active site. The resting state of thrombin, also called slow-thrombin or E*, seems to feature a more exposed N-terminus$^{(Ile16)}$ than ligand-bound thrombin.[8] Another serine protease Factor VIIa is several orders of a magnitude less active in the absence of its cofactor, tissue factor.[7] Tissue factor converts ligand-free Factor VIIa into its active conformation by an allosteric transition, which can be measured directly by chemical carbamylation of the exposed α-amino group of Ile16 at the N-terminus. Reactivity of the N-terminus$^{(Ile16)}$ to carbamylation is determined by the distribution between a state with the N-terminus$^{(Ile16)}$ inserted into the activation pocket and a state with an exposed N-terminus$^{(Ile16)}$. The presence of trypsin-like serine proteases in resting states in the absence of bound ligands has been corroborated by crystal structures of free enzymes, exhibiting a partial collapse of the 215−217 β-strand into the active site and a disruption of the oxyanion-hole.[9] It was recently suggested that the distorted conformations observed in mutants of thrombin are distributed along a continuum and that ligand binding rectifies these molecules to the active conformation, as evidenced by large thermodynamic differences in the binding reactions.[10] However, a relationship between the extent of these thermodynamic

Received: May 7, 2012
Revised: August 16, 2012
Published: September 5, 2012

dx.doi.org/10.1021/bi3005957 | *Biochemistry* 2012, 51, 7804−7811

differences and the exposure of the N-terminus$^{(Ile16)}$ has not been demonstrated.

Activation of plasminogen into plasmin, which degrades the extracellular matrix and facilitates dissemination of cancer cells, is catalyzed by urokinase-type plasminogen activator (uPA).[11,12] Its role in cancer spread has implicated uPA as a therapeutic target. From this point of view, improved understanding of the regulatory mechanisms of allosteric serine proteases is important in the development of new strategies for therapeutic intervention. The catalytic domain represented by the B-chain of uPA is covalently linked to the A-chain by the Cys1-Cys122 disulfide-bond. Cys1 is located C-terminally to the intradomain linker, the epidermal growth factor-like domain and the kringle domain. Specifically, the epidermal growth factor-like domain is responsible for association of uPA to the cell surface by direct noncovalent interaction with the uPA receptor, uPAR.[12] Active uPA associates with a serpin, known as plasminogen activator inhibitor-1 (PAI-1), and forms an inhibited covalent complex.[13]

The monoclonal antibody, mU3 was previously shown to inhibit plasminogen activation catalyzed by murine uPA (muPA).[14] Here we report that mU3 binds to an exosite of muPA in the 37- and 70-loops, a site homologous to exosite I of thrombin. We have addressed how the exosite in the 37- and 70-loops is coupled to events in the active site, the overall conformation of the enzyme, and exposure of the N-terminus$^{(Ile16)}$. Binding of mU3 to the 37- and 70-loops and inhibitors to the active site promoted the conversion from partially inactive distorted states to the active state. Using the active site binding peptidic inhibitor mupain-1−16,[15] we establish for the first time a relationship between the large thermodynamic differences of ligand binding reactions and the increased exposure of the N-terminus$^{(Ile16)}$ in distorted relative to less distorted states of serine proteases.

MATERIALS AND METHODS

Monoclonal Antibodies and Peptides. The generation and characterization of mU3 were described previously.[14] The peptide mupain-1−16 (CPAYS(L-3-(*N*-amidino-4-piperidyl)-alanine)YLDC) was prepared by solid-phase synthesis.[15]

Transfection of HEK293 6E Suspension Cells. Different cDNAs encoding full-length muPA, muPA$^{(16-243)}$, and site-directed mutants were cloned into the pTT5 or pCDNA3.1 vectors. All variants contained six histidines at the C-terminus. The muPA$^{(16-243)}$ variants contained a C122A mutation. The cDNAs were transfected into human embryonic kidney 293 (HEK293) 6E suspension cells and cultured in a humidified 5% CO_2 incubator at 37 °C. The media used was F17 containing 4 mM L-glutamine, 0.1% FP68, 100 units/mL penicillin, 100 units/mL streptomycin, 25 μg/mL G418. Linear polyethyleneimine (PEI) (2.2 mg), cDNA (1.1 mg), and PBS (110 mL) were preincubated for 15 min and added to 1 L of culture with a density of 1×10^6 cells/mL. Tryptone N1 (0.5%) was added to the culture 24 h post-transfection. Culturing was continued for six days before harvesting the conditioned media.

Protein Purification. Full-length tc-muPA and variants were purified from conditioned media of transiently transfected HEK293 6E cells. Briefly, C-terminally 6xhistidine-tagged proteins were captured on nickel-Sepharose, eluted with imidazole, and purified further using Superdex 75 size-exclusion chromatography.

Plasminogen Activation Assays. Various concentrations of mU3 (0−25 nM) were incubated with full-length tc-muPA, muPA$^{(16-243)}$, or mutants hereof (0.5 nM) and preincubated for 30 min at 25 °C in HBS (10 mM Hepes pH 7.4, 140 mM NaCl, 0.1% BSA). Next, the reaction was initiated by addition of 0.5 μM human plasminogen and 0.5 mM plasmin substrate H-D-Val-Leu-Lys-*p*-nitroanilide (S-2251). S-2251 hydrolysis was monitored at 37 °C for the parabolic increase in absorbance at 405 nm. To determine the velocity of plasminogen activation, the data were transformed to plot Δ405/Δtime on the ordinate and time on the abscissa.[16] Velocities were calculated from the time interval 5−20 min of these plots and used for calculations of IC_{50}.

Amidolytic Assay of muPA Proteolytic Activity. The velocity of muPA catalyzed hydrolysis of H-D-Glu-Gly-Arg-*p*-nitroanilide (S-2444) was measured at 37 °C in HBS. K_m and K_i were calculated as described previously.[15]

Surface Plasmon Resonance Measurements. To determine the equilibrium binding constant (K_D), the association rate constant (k_{on}) and dissociation rate constant (k_{off}) for mU3 binding to muPA and variants, surface plasmon resonance analyses were performed on a Biacore T200 instrument (Biacore, Uppsala, Sweden). A CM5 chip was coupled with polyclonal rabbit anti-mouse IgG from the Mouse Antibody Capture kit from GE-Healthcare through amine coupling: A concentration of 30 μg/mL anti-mouse IgG in immobilization buffer (10 mM sodium acetate, pH 5.0) was injected during 7 min at a flow rate of 10 μL/min until a level of 14 000 response units (RU) was reached, followed by surface blocking with ethanolamine. The monoclonal antibody (mU3) in running buffer (30 mM Hepes pH 7.4, 135 mM NaCl, 1 mM EDTA) + 1% BSA was injected at a flow rate of 5 μL/min for 180 s until a capture level of ∼1100 RU was reached. A flow cell without injection of mU3 was used as the reference. A dilution series of muPA variants (0−100 nM) in running buffer + 1% BSA was injected at a flow rate of 30 μL/min during 60 s at 25 °C. Subsequently, the dissociation was monitored for 220 s. Binding of mupain-1−16 to muPA variants was measured by immobilization of 20 000 RU of an anti-histidine tag antibody onto a CM5 chip as described above and used to capture 3000 RU of muPA or variants. Next, mupain-1−16 (0−1000 nM) was injected in running buffer containing 0.1% BSA at a flow rate of 30 μL/min during 60 s at 25 °C. A flow cell without binding of muPA was used as reference and the response without mupain-1−16 was subtracted from each curve. Kinetic constants (k_{on} and k_{off}) were calculated using the Biacore Evaluation Software to generate a 1:1 kinetic fit. Although some data sets could be fitted better to a two-state model, the calculated data were similar when using a 1:1 model. All data were therefore fitted to a 1:1 model. The K_D values were calculated as k_{off}/k_{on}.

Carbamylation Assay. To analyze the effect of mU3 and mupain-1−16 on the carbamylation rate of the N-terminal$^{(Ile16)}$ α-amino group in different muPA variants, 0.5 μM enzyme was preincubated with or without mU3 (1 μM) or mupain-1−16 (1 μM) in HS buffer (10 mM Hepes pH 7.4, 140 mM NaCl) + 0.1% PEG 8000 at 22 °C for 30 min. After preincubation, potassium cyanate (0.2 M) or HS buffer +0.1% PEG 8000 was added and incubated at 22 °C for 0, 30, 60, 120, 180, and 300 min. To stop the carbamylation reaction, each of the mixtures was diluted 100-fold in HBS, and mU3 or mupain-1−16 was allowed to dissociate for 2 h at 22 °C. The residual activity was determined in the presence of S-2444 (750 μM) by measuring the rate of hydrolysis at 405 nm for 1 h at 37 °C in a microplate reader.

Isothermal Titration Calorimetry. All isothermal titration calorimetry (ITC) experiments were performed on a MicroCal VP-ITC instrument equilibrated to a temperature of 25 °C. The muPA variants were dialyzed into a buffer of 20 mM sodium phosphate, pH 7.4, 140 mM NaCl. The peptide mupain-1−16 was dissolved in the same buffer and the concentration was determined using the extinction coefficient calculated using Protparam located at http://us.expasy.org/tools/protparam.html. In all cases, experiments were designed to provide a fully saturated titration profile with enough signal and curvature to allow precise determination of thermodynamic parameters. The concentration of muPA variant used in the ∼1.4 mL sample cell was 0.5−2 μM, depending on the affinity of the ligand. Titrations were performed by injecting 10−12 μL of the ligand until the total syringe volume of 296 μL was spent. The equilibrium association constant K_A and the molar reaction enthalpy ΔH were calculated by fitting the integrated titration peaks using a one-binding-site model in the ITC ORIGIN7 program package. The following formulas for Gibbs energy ΔG were used to analyze the measured energies.

$$\Delta G = -RT \ln K_A \quad (1)$$

$$\Delta G = \Delta H - T\Delta S \quad (2)$$

in which R is the gas constant and T is the absolute temperature. ΔS, the entropic change during the reaction, was calculated by combining eqs 1 and 2 using the measured K_A and ΔH. Titration of ligand into buffer was performed to obtain buffer correction.

Determination of Second Order Rate Constants for Binding of muPA to PAI-1. Full-length tc-muPA or muPA$^{(16-243)}$ (0.25 nM) were mixed with 100 nM mU3 or HBS and incubated for 30 min at 25 °C. At time point t = 0 min, the reaction was mixed with a dilution series of murine PAI-1 (0−500 nM). The absorbance at 405 nm (A_{405}) was recorded for 120 min in the presence of 3 mM or 6 mM S-2444 for full-length tc-muPA or muPA$^{(16-243)}$, respectively. The k_{obs} values for each PAI-1 concentration were determined by fitting the progress curves to the single-exponential function (eq 3).

$$[P]_t = [P]_0 + [P]_\infty(1 - e^{-k_{obs}t}) \quad (3)$$

where $[P]_t$, $[P]_0$, and $[P]_\infty$ are the product concentrations at time t, time zero, and time infinite, respectively, proportional to the measured A_{405} values. The calculated k_{obs} values were then plotted on the ordinate and the PAI-1 concentrations on the abscissa and the K_D and k_{lim} values were determined by fitting the data to eq 4.

$$k_{obs} = k_{lim}[\text{PAI-1}]_0 \Big/ \left[K_D\left(1 + \frac{[\text{S-2444}]}{K_m}\right) + [\text{PAI-1}]_0\right] \quad (4)$$

The second-order rate constant k_2 was calculated as k_{lim}/K_D.

RESULTS

The Epitope of mU3 Is Located in the 37- and 70-Loops. A total of 29 site-directed alanine substitution mutants of full-length tc-muPA were prepared to identify the epitope of the monoclonal antibody, mU3.[14] The plasminogen activation activities of the full-length tc-muPA mutants G37cA, P37eA, P38A, S74A, Y76A, and N77A were not inhibited by mU3 (data not shown). Contrary, mU3 inhibited the plasminogen activation activities of full-length tc-muPA E23A, Q35A, N37A, K37aA, G37bA, S37dA, K41A, Q60aA, K72A, E73A, S75A, P78A, Y93A, E96A, Y99A, T110A, S110aA, K143A, E146A, Y149A, L150A, K153A, and R217A (data not shown). The inhibition of these 23 mutants by mU3 was indistinguishable from the inhibition of full-length tc-muPA, suggesting the epitope of mU3 to consist of amino acid residues in the 37- and 70-loops. To further validate the plasminogen activation data, we used surface plasmon resonance analysis to quantitate mU3 binding to variants mutated within and around the epitope. Binding to mU3 was diminished for the mutants of full-length tc-muPA, G37cA, P37eA, P38A, S74A, Y76A, and N77A (Table 1 and Figure 1). Hence, the plasminogen activation activities of these six mutants were not inhibited by mU3 as they did not bind the antibody at the concentrations used in the assay. None of the mutations completely abolished the binding. The most compromised mutant was G37cA (Figure 1B and Table 1). The decreased binding of mU3 to the mutants consistently resulted from an increase in k_{off} (Table 1). Full-length tc-muPA N37A, K37aA, G37bA, S37dA, K72A, P78A, Y149A, and K153A were shown to bind to mU3 with similar affinities as full-length tc-muPA (Figure 1C). Hence, mU3 binds to an epitope in the 37- and 70-loops (Figure 1C). Interestingly, binding of mU3 to the 37-loop seems to depend on a certain conformation rather than side-chain interactions, as only mutation of Gly and Pro residues affected binding to the 37-loop.

Table 1. Binding of mU3 to Full-Length tc-muPA and Variants Determined by Surface Plasmon Resonance Analysis[a]

	$k_{on}\cdot10^{-5}$ ($M^{-1}\cdot s^{-1}$)	$k_{off}\cdot10^{4}$ (s^{-1})	K_D (nM)
full-length tc-muPA	11.4 ± 1.5	4.8 ± 0.6	0.4 ± 0.1
muPA$^{(16-243)}$	7.0 ± 1.0	5.1 ± 1.1	0.7 ± 0.2[b]
full-length tc-muPA G37cA	6.4 ± 4.4	276 ± 78	129 ± 89[b]
full-length tc-muPA P37eA	2.7 ± 0.4	91 ± 13	34 ± 8[b]
full-length tc-muPA P38A	3.4 ± 2.1	39 ± 4	15 ± 9[b]
full-length tc-muPA S74A	3.9 ± 1.4	12 ± 5	3.1 ± 1.7[b]
full-length tc-muPA Y76A	3.8 ± 1.6	25 ± 8	7.1 ± 1.9[b]
full-length tc-muPA N77A	6.4 ± 2.7	20 ± 3	3.4 ± 1.3[b]

[a]Data are the average ± standard deviations for three independent determinations. Each determination was calculated from sensorgrams derived from five different concentrations of the given variant (as demonstrated in Figure 1A). [b]Significantly different from the value for full-length tc-muPA ($p < 0.01$) − Student's t test.

The Antibody mU3 Decreases K_m for S-2444 Hydrolysis. The truncated mutant, muPA$^{(16-243)}$ consists of the B-chain of murine uPA. As demonstrated below, muPA$^{(16-243)}$ exists in a distorted state, as its N-terminus is more exposed than in full-length tc-muPA. In all our experiments, mU3 restored the active state of muPA$^{(16-243)}$ (see below). The amidolytic activity of full-length tc-muPA was not affected by mU3, while the amidolytic activity of muPA$^{(16-243)}$ was dose-dependently increased up to maximally 2-fold (Figure 2A). Furthermore, mU3 improved the affinity of the substrate S-2444 for the active site, as K_m for muPA$^{(16-243)}$ was decreased from 5 ± 0.7 mM in the absence of mU3 to the level of full-length tc-muPA at 2.4 ± 0.2 mM in the presence of mU3 (Figure 2B and Table 2). Moreover, k_{cat} was not affected by mU3, but remained constantly at approximately 90 s^{-1} for both full-length tc-muPA and muPA$^{(16-243)}$ (Figure 2B). Notably, mU3 dose-dependently inhibited plasminogen

dx.doi.org/10.1021/bi3005957 | Biochemistry 2012, 51, 7804−7811

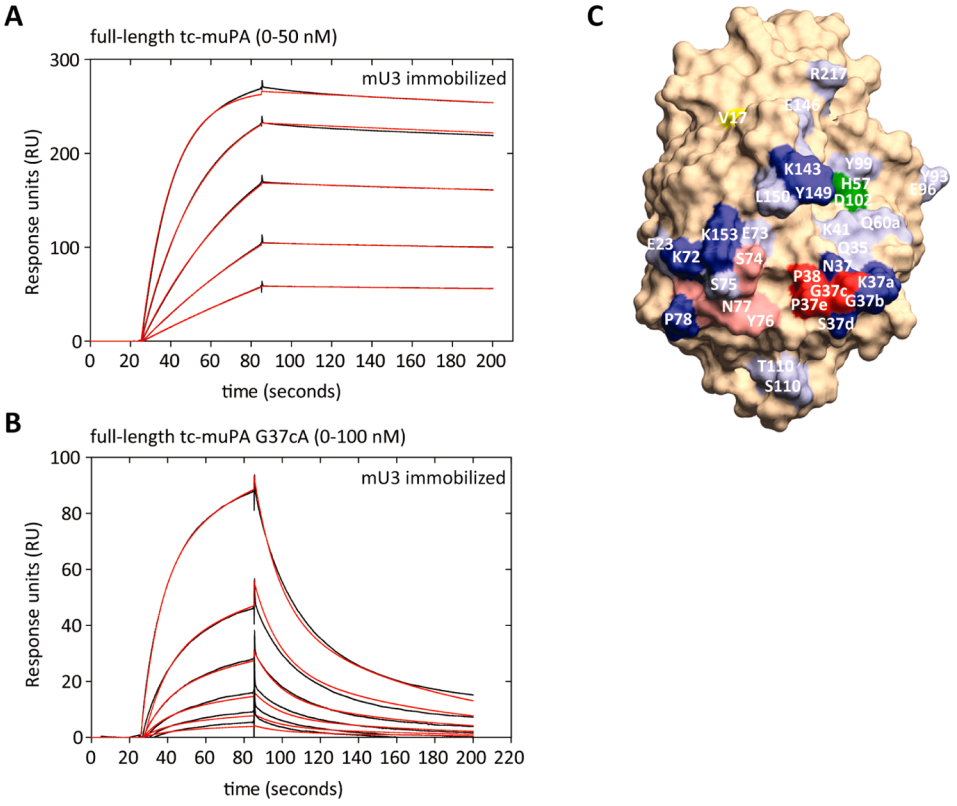

Figure 1. The epitope of mU3 on muPA. Surface plasmon resonance sensorgrams for binding of mU3 to full-length tc-muPA (A) and full-length tc-muPA G37cA (B). Fits are shown in red and experimental curves in black. (C) The epitope of mU3. Substitution of light-red and red residues to alanine resulted in approximately 10-fold and more than 60-fold reduction in binding, respectively. Val17 in yellow specifies the activation pocket. His57 and Asp102 in green are located in the active site. Residues in blue could be mutated to alanine without compromising mU3 binding to muPA. Residues in light blue could be mutated to alanine without compromising mU3 inhibition of the plasminogen activation activity of the mutant. The structure of the muPA catalytic domain was homology modeled from a crystal structure of human uPA (PDB entry: 2NWN).

activation by both full-length tc-muPA and muPA$^{(16-243)}$ with an IC_{50} of approximately 0.3 nM (Figure 2C). These data indicate that mU3 restores the affinity of the active site of muPA$^{(16-243)}$ for S-2444 and sterically inhibits plasminogen activation.

A Peptidic Substrate and Active Site Inhibitors have Lower Affinity for Distorted muPA Variants than for Full-Length tc-muPA. K_m for hydrolysis of S-2444 was 2-fold higher for muPA$^{(16-243)}$ than for full-length tc-muPA (Table 2). Mutants with substitutions located close to the epitope of mU3 and the oxyanion hole were analyzed to identify more distorted variants. The mutants muPA$^{(16-243)}$ F40Y and muPA$^{(16-243)}$ E137A were selected for analysis, as their K_m values for S-2444 hydrolysis were higher than for muPA$^{(16-243)}$ (Table 2). Hence, it was hypothesized that mutations away from the active site that increased K_m for S-2444 hydrolysis would also induce conformational distortion and as demonstrated below, exposure of the N-terminus$^{(Ile16)}$. Inhibition of muPA$^{(16-243)}$ with the active site antagonists, *p*-aminobenzamidine (*p*AB), amiloride and mupain-1−16 showed K_i values 2−3 fold higher than the K_i values of the same inhibitors for full-length tc-muPA (Table 2). For the mutants, muPA$^{(16-243)}$ F40Y and muPA$^{(16-243)}$ E137A, the difference to full-length tc-muPA was even more drastic, with increases in the K_i values of 5- to 10-fold. These data demonstrated a decreased affinity of distorted states of muPA for the S-2444 substrate and for active site inhibitors.

The Affinity of Distorted Mutants for Inhibitors Is Restored by mU3. Because mU3 improved the binding of S-2444 to the active site of muPA$^{(16-243)}$, we now continued to measure whether this effect occurred for active site inhibitors. All three inhibitors tested, *p*AB, amiloride and mupain-1−16, had a 2−3 fold lower K_i for muPA$^{(16-243)}$ in the presence of mU3 than in its absence, corresponding to the values for the full-length tc-muPA (Table 2). Similar effects occurred for the F40Y and E137A mutants of muPA$^{(16-243)}$. Based on these data, we conclude that mU3 restores the active state of the distorted muPA mutants.

Binding of PAI-1 to muPA$^{(16-243)}$ Is Slower than to Full-Length tc-muPA and mU3 Reduces the Rate of Binding. We measured the second-order rate constants for binding of murine PAI-1 to full-length tc-muPA and muPA$^{(16-243)}$ (Figure 3). First, the second-order rate constant was 2−3-fold slower for muPA$^{(16-243)}$ than for full-length tc-muPA. The reason for this is probably that muPA$^{(16-243)}$ is distorted. Second, mU3 decreased the second-order rate constant by 8-fold for full-length tc-muPA and 5-fold for muPA$^{(16-243)}$. From these data we deduce that mU3 delays the binding of PAI-1 to muPA, probably by steric hindrance.

mU3 and mupain-1−16 Mediate Insertion of the N-Terminus$^{(Ile16)}$ into the Activation Pocket. We now measured the rates of inactivation of full-length tc-muPA and muPA$^{(16-243)}$ during modification of the exposed α-amino group of Ile16 by chemical carbamylation. The rate of inactivation by carbamylation is proportional to the fraction of the time the N-terminus$^{(Ile16)}$ is solvent exposed versus the time in which it is salt-bridged to Asp194. The rate of

dx.doi.org/10.1021/bi3005957 | *Biochemistry* 2012, 51, 7804−7811

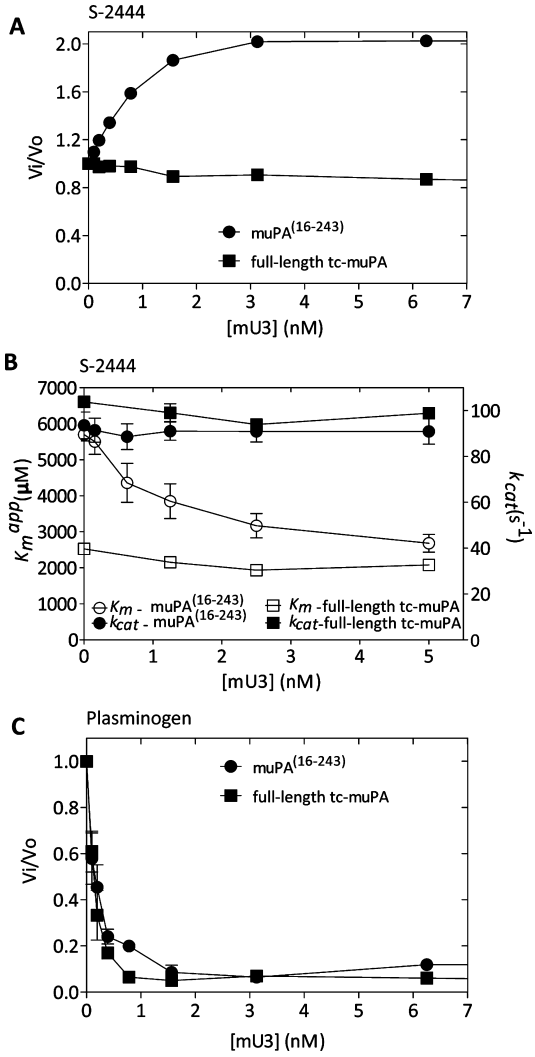

Figure 2. The K_m for S-2444 hydrolysis is decreased and plasminogen activation is inhibited by mU3. (A) Hydrolysis of S-2444 (0.75 mM) measured for full-length tc-muPA and muPA$^{(16-243)}$ (2 nM) at the indicated concentrations of mU3. (B) K_m and k_{cat} for hydrolysis of S-2444 by full-length tc-muPA and muPA$^{(16-243)}$ measured at the indicated concentrations of mU3. (C) Activation of human plasminogen (0.5 μM) measured for full-length tc-muPA and muPA$^{(16-243)}$ (0.5 nM) using S-2251 (0.5 mM) and mU3 at the indicated concentrations. All measurements are the average ± standard deviations of at least three independent determinations.

carbamylation was found to be faster for muPA$^{(16-243)}$ than for full-length tc-muPA (Table 3 and Figure 4). Hence, the N-terminus$^{(Ile16)}$ of muPA$^{(16-243)}$ is more exposed than in full-length tc-muPA. Next, it was demonstrated that mU3 decreased the carbamylation rate for muPA$^{(16-243)}$ to the rate measured for full-length tc-muPA (Table 3). Similarly, insertion of the N-terminus$^{(Ile16)}$ was promoted by mupain-1−16, as the rate of carbamylation decreased upon binding of mupain-1−16 to muPA$^{(16-243)}$ (Figure 4A). Hence, mU3 and mupain-1−16 promote insertion of the N-terminus$^{(Ile16)}$ into the activation pocket. To demonstrate that the N-terminus$^{(Ile16)}$ is more exposed in more distorted mutants, we determined the carbamylation rates of the muPA$^{(16-243)}$ mutants, F40Y and E137A. These two mutants had even more exposed N-termini$^{(Ile16)}$ than muPA$^{(16-243)}$, again demonstrating more distorted states in these variants (Figure 4B).

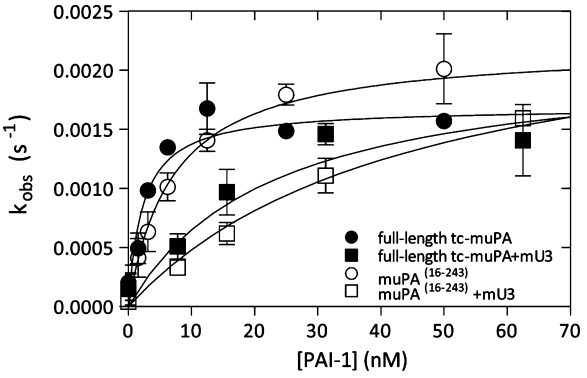

Figure 3. Binding of murine PAI-1 to muPA and muPA$^{(16-243)}$ is delayed by mU3. The second-order rate constants for reaction with murine PAI-1 were: full-length tc-muPA; (1.75 ± 0.48)·10^6 M^{-1}·s^{-1}, full-length tc-muPA+mU3; (2.93 ± 1.41)·10^5 M^{-1}·s^{-1}, muPA$^{(16-243)}$; (6.85 ± 2.28)·10^5 M^{-1}·s^{-1}, muPA$^{(16-243)}$+mU3; (1.29 ± 0.47)·10^5 M^{-1}·s^{-1}. All measurements are the average ± standard deviations of at least three independent determinations.

Table 3. Rates (min^{-1}) of Inactivation by Chemical Carbamylation[a]

	ligand-free	+mU3	+mupain-1−16
full-length tc-muPA	1.5 ± 0.7	1.0 ± 0.7	0.2 ± 0.1
muPA$^{(16-243)}$	9.6 ± 1.0[b]	1.2 ± 0.7	0.5 ± 0.4

[a]Data are the average ± standard deviations of three independent determinations. [b]Significantly different from the value determined for full-length tc-muPA (p < 0.0003) − Student's t test.

Large Thermodynamic Differences in the mupain-1−16 Binding Reaction Distinguish Distorted Mutants of muPA. The kinetic data presented in Table 2 indicate that mU3 restores the active state of muPA$^{(16-243)}$, muPA$^{(16-243)}$ F40Y, and muPA$^{(16-243)}$ E137A. Like mU3, the active site inhibitor, mupain-1−16 is assumed to restore the active state of muPA mutants in distorted states. To measure the extent of

Table 2. K_m for S-2444 Hydrolysis and K_i for Inhibition by Amiloride, *p*AB and mupain-1−16 for muPA Variants[a]

	K_m (mM) S-2444		K_i (μM) amiloride		K_i (μM) *p*AB		K_i (nM) mupain-1−16	
	−mU3	+mU3	−mU3	+mU3	−mU3	+mU3	−mU3	+mU3
full-length tc-muPA	2.4 ± 0.2	2.1 ± 0.1	6 ± 1	9 ± 1	31 ± 1	27 ± 3	39 ± 10	30 ± 15
muPA$^{(16-243)}$	5.0 ± 0.7[b]	2.7 ± 0.4	16 ± 1[b]	9 ± 2	71 ± 9[b]	32 ± 11	90 ± 1[b]	30 ± 1
full-length tc-muPA F40Y	4.5 ± 0.2[b]	2.4 ± 0.3	14 ± 3[b]	12 ± 2	84 ± 11[b]	55 ± 10	110 ± 7[b]	55 ± 14
muPA$^{(16-243)}$ F40Y	11.6 ± 0.9[b]	4.4 ± 0.4[b]	53 ± 12[b]	22 ± 7[b]	150 ± 11[b]	79 ± 10[b]	213 ± 38[b]	78 ± 4[b]
muPA$^{(16-243)}$ E137A	8.0 ± 0.7[b]	6.9 ± 0.1[b]	74 ± 12[b]	19 ± 2[b]	318 ± 39[b]	74 ± 10[b]	490 ± 30[b]	76 ± 6[b]

[a]All data are the average ± standard deviations of at least three independent determinations. A saturating concentration of mU3 (25 nM) was used. [b]Significantly different from the corresponding value determined for full-length tc-muPA (p < 0.004) − Student's t test.

dx.doi.org/10.1021/bi3005957 | *Biochemistry* 2012, 51, 7804−7811

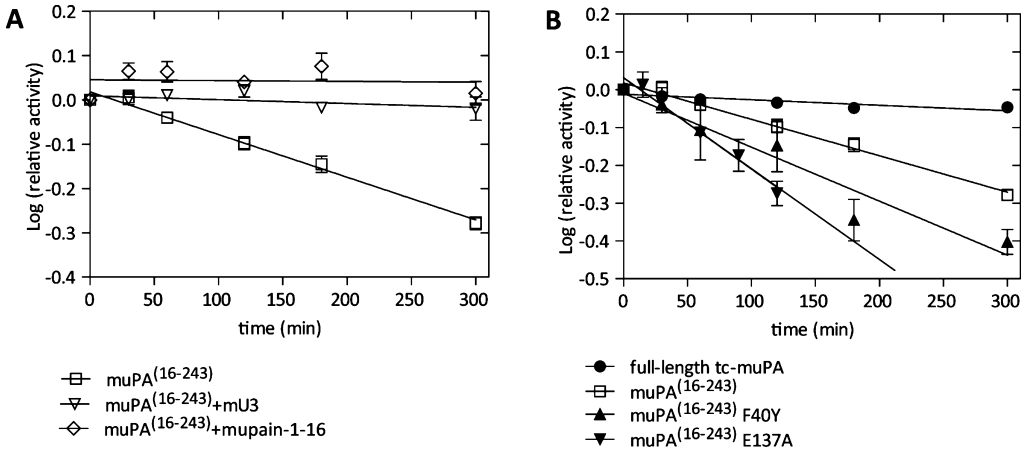

Figure 4. Carbamylation of muPA variants. (A) Time-dependent inactivation by carbamylation of muPA$^{(16-243)}$ in the presence and absence of mU3 or mupain-1−16. (B) Carbamylation of full-length tc-muPA, muPA$^{(16-243)}$, muPA$^{(16-243)}$ F40Y and muPA$^{(16-243)}$ E137A. All measurements are the average ± standard deviations of at least three independent determinations. The carbamylation rates for muPA$^{(16-243)}$ F40Y was 14.2 ± 1.7 min^{-1} and 24.2 ± 4.0 min^{-1} for muPA$^{(16-243)}$ E137A. All other rates are shown in Table 3.

Table 4. Thermodynamic Parameters for Binding of mupain-1−16 to muPA Variants Determined by ITC and k_{on}, k_{off}, and K_D Determined by Surface Plasmon Resonance Analyses[a]

	isothermal titration calorimetry				surface plasmon resonance		
	ΔH (kJ/mol)	$T\Delta S$ (kJ/mol)	ΔG (kJ/mol)	K_D (nM)	$k_{on}\cdot10^{-5}$ ($M^{-1}\cdot s^{-1}$)	$k_{off}\cdot10^{4}$ (s^{-1})	K_D (nM)
full-length tc-muPA	−39 ± 4	4 ± 3	−43 ± 1	29 ± 6	1.7 ± 0.2	59 ± 2	35 ± 3
muPA$^{(16-243)}$	−61 ± 5[b]	−18 ± 4[b]	−44 ± 1	25 ± 7	1.3 ± 0.1	57 ± 14	46 ± 10
full-length tc-muPA +mU3	−42 ± 6	2 ± 6	−44 ± 1	25 ± 2	n.d.	n.d.	n.d.
muPA$^{(16-243)}$ +mU3	−43 ± 2	1 ± 2	−44 ± 1	23 ± 5	n.d.	n.d.	n.d.
muPA$^{(16-243)}$ F40Y	−64 ± 2[b]	−27 ± 1[b]	−41 ± 1[b]	81 ± 19[b]	1.3 ± 0.4	123 ± 35[c]	94 ± 6[c]
muPA$^{(16-243)}$ E137A	−71 ± 3[b]	−29 ± 2[b]	−42 ± 1	52 ± 26	0.9 ± 0.1[c]	68 ± 2	77 ± 13[c]

[a]All data are the average ± standard deviations of at least three independent determinations. n.d.: Data were not determined. For each surface plasmon resonance determination, six different concentrations of mupain-1−16 were used (see Figure S1). [b]Significantly different from the value determined for full-length tc-muPA ($p < 0.01$) − Student's t test. [c]Significantly different from the value determined for muPA$^{(16-243)}$ ($p < 0.03$) − Student's t test.

conformational distortion in different muPA mutants we used isothermal titration calorimetry (ITC) and quantitated the ordering occurring in a distorted mutant when its active state is restored through binding of mupain-1−16. Hence, a more negative ΔH reflects formation and disruption of more noncovalent bonds and a more negative $T\Delta S$ parameter reflects more ordering upon binding of mupain-1−16. The ΔH for binding of mupain-1−16 is more negative for muPA$^{(16-243)}$ than for full-length tc-muPA, indicating the formation of more noncovalent interactions on a net basis (Table 4 and Figure S1). Because of a compensatory more negative $T\Delta S$, the ΔG for binding of mupain-1−16 was comparable for full-length tc-muPA and muPA$^{(16-243)}$. The K_D values determined by ITC did not deviate measurably from the K_D values determined by surface plasmon resonance analysis (Table 4 and Figure S1). The negative $T\Delta S$ for binding of mupain-1−16 to muPA$^{(16-243)}$ suggests that this variant is flexible but becomes more ordered upon binding of mupain-1−16. Interestingly, we observed that ΔH and $T\Delta S$ for binding to mupain-1−16 were alike for full-length tc-muPA and muPA$^{(16-243)}$ when they were in complex with mU3 (Table 4). Based on this, it appears that mU3 restores the active state of muPA$^{(16-243)}$, which seems to resemble the state assumed by full-length tc-muPA. The $T\Delta S$ value for binding to mupain-1−16 was more negative for muPA$^{(16-243)}$ F40Y and muPA$^{(16-243)}$ E137A than for muPA$^{(16-243)}$, indicating that these two mutants are in even more distorted states but become ordered upon binding to the peptide. For muPA$^{(16-243)}$ F40Y, the k_{on} for binding to mupain-1−16 was similar to muPA$^{(16-243)}$, whereas the k_{off} rate was significantly increased. For the muPA$^{(16-243)}$ E137A mutant, the k_{on} for binding to mupain-1−16 was lower than for muPA$^{(16-243)}$, whereas the k_{off} rates were comparable. The large differences in the thermodynamic parameters (ΔH and $T\Delta S$) for binding to mupain-1−16 among the mutants were not a result of changes in the ΔG for which the variation among the tested mutants was about 3% (Table 4).

DISCUSSION

In this study, we report new data about the allosteric communication between an antibody epitope in the 37- and 70-loops, the N-terminus$^{(Ile16)}$ in the activation pocket, and inhibitors or substrates in the active site of muPA. Overall, our data contribute to a functional elucidation of the interconversion between distorted states of uPA and its active conformation.

It is tempting to compare the epitope of mU3 to exosite I of thrombin, which is also located in the 37- and 70-loops. Exosite I mediates allosteric signals from cofactors, inhibitors and substrates to the active site of thrombin.[2] However, evidence for a biological role of the 37- and 70-loops of uPA remains to be identified. When thrombomodulin binds to exosite I of thrombin, the ability to cleave fibrinogen is lost and the

dx.doi.org/10.1021/bi3005957 | Biochemistry 2012, 51, 7804−7811

specificity switches toward cleavage of protein C.[17] Exosite I regulates the conformation of thrombin through binding to different ligands, all inducing the active conformation of the enzyme. The mechanism through which mU3 restores the active state of distorted muPA variants could to some extent be analogous to that of thrombin ligands binding to exosite I.

The current work has led to new fundamental knowledge on the relationship between the thermodynamic events occurring upon binding of ligands to muPA. Other serine proteases exhibiting similar distorted conformations may be regulated by the same mechanisms. As it was suggested previously, a continuum of distorted structures seems to be represented in different mutants and ligand-bound states of thrombin.[10] First, as observed when binding ligands to the active site or exosite I of thrombin,[10,18] we measured a more negative ΔH and a more negative $T\Delta S$ for binding of mupain-1−16 to muPA$^{(16-243)}$ and its F40Y and E137A mutants than for binding to full-length tc-muPA. Both ΔH and $T\Delta S$ became more negative, when the N-terminus$^{(Ile16)}$ was more exposed as measured by chemical carbamylation of Ile16, whereas ΔG was largely unchanged (Figure 5). The decrease in $T\Delta S$ for mupain-1−16 binding to

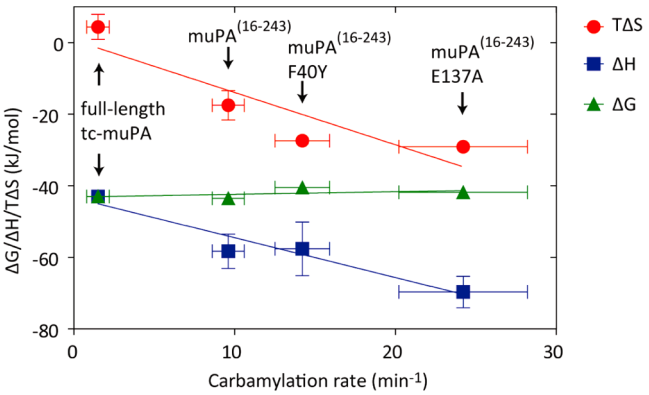

Figure 5. The rate of N-terminal$^{(Ile16)}$ carbamylation of muPA variants increases when ΔH and ΔS for mupain-1−16 binding become more negative. Data used for the plot are shown in Figure 4 and Tables 3 and 4.

mutants in more distorted states reflects the conversion from distorted states to the active state. Hence, a mutant in a more distorted state undergoes more extensive ordering upon binding of mupain-1−16 in order to assume the active state. The more negative $T\Delta S$ for binding of mupain-1−16 to muPA$^{(16-243)}$ F40Y and E137A than for binding to muPA$^{(16-243)}$ occurs as these mutants are in even more distorted states and undergo more extensive ordering. Consequently, binding of mupain-1−16 to the active site of muPA induces the active conformation and the N-terminus$^{(Ile16)}$ is inserted into the activation pocket. Induction of the active conformation upon binding to mupain-1−16 decreases ΔH depending on the number of noncovalent bonds that must be disrupted and formed for the transition to occur. This lowering of ΔH compensates for the drop in $T\Delta S$, since the affinities (ΔG) of the muPA mutants for mupain-1−16 are similar. Based on these data, we suggest that the larger thermodynamic differences for the binding of ligands to distorted states of serine proteases, as demonstrated here for muPA, seem to correlate with increased duration of solvent exposure of the N-terminus$^{(Ile16)}$. One of the most important arguments supporting these conclusions is that muPA$^{(16-243)}$ is completely rectified into the active state by mU3, which promotes insertion of the N-terminus$^{(Ile16)}$ and decreases the ordering associated with binding of active site inhibitors and substrates. Accordingly, the distorted muPA mutants bind mupain-1−16 by an induced-fit mechanism, in which the enzyme changes conformation to fit the ligand.

■ ASSOCIATED CONTENT

Ⓢ Supporting Information

ITC graphs and surface plasmon resonance sensorgrams showing the binding of mupain-1−16 to different muPA variants are presented in Figure S1. This material is available free of charge via the Internet at http://pubs.acs.org.

■ AUTHOR INFORMATION

Corresponding Author

*Address: Department of Molecular Biology and Genetics, Aarhus University, Gustav Wieds Vej 10 C, DK-8000 Aarhus C, Denmark. Tel: (+45) 8715 4907. E-mail: hps@mb.au.dk.

Funding

This work was supported by grants from the Danish Cancer Society (DP 07043, DP 08001); the Danish National Research Foundation (26-331-6); the Danish Research Agency (272-06-0518); the Novo Nordisk Foundation (R114-A11382); and the Lundbeck Foundation.

Notes

The authors declare no competing financial interests.

■ ABBREVIATIONS USED

uPA, urokinase-type plasminogen activator; PAI-1, plasminogen activator inhibitor-1; muPA, murine uPA; tc, two-chain; HEK, human embryonic kidney; PEI, polyethyleneimine; S-2444, H-D-Glu-Gly-Arg-*p*-nitroanilide; S-2251, H-D-Val-Leu-Lys-*p*-nitroanilide; RU, response units; ITC, isothermal titration calorimetry; pAb, *p*-aminobenzamidine

■ ADDITIONAL NOTE

[a]Numbering is according to the chymotrypsin template.[19]

■ REFERENCES

(1) Hedstrom, L. (2002) Serine protease mechanism and specificity. *Chem. Rev. 102*, 4501−4524.

(2) Huntington, J. A. (2012) Thrombin plasticity. *Biochim. Biophys. Acta 1824*, 246−252.

(3) Lechtenberg, B. C., Johnson, D. J., Freund, S. M., and Huntington, J. A. (2010) NMR resonance assignments of thrombin reveal the conformational and dynamic effects of ligation. *Proc. Natl. Acad. Sci. U. S. A. 107*, 14087−14092.

(4) Jing, H., Babu, Y. S., Moore, D., Kilpatrick, J. M., Liu, X. Y., Volanakis, J. E., and Narayana, S. V. (1998) Structures of native and complexed complement factor D: implications of the atypical His57 conformation and self-inhibitory loop in the regulation of specific serine protease activity. *J. Mol. Biol. 282*, 1061−1081.

(5) Narayana, S. V., Carson, M., el-Kabbani, O., Kilpatrick, J. M., Moore, D., Chen, X., Bugg, C. E., Volanakis, J. E., and DeLucas, L. J. (1994) Structure of human factor D. A complement system protein at 2.0 Å resolution. *J. Mol. Biol. 235*, 695−708.

(6) Gohara, D. W., and Di Cera, E. (2011) Allostery in trypsin-like proteases suggests new therapeutic strategies. *Trends Biotechnol. 29*, 577−585.

(7) Persson, E., and Olsen, O. H. (2010) Current status on tissue factor activation of factor VIIa. *Thromb. Res. 125*, S11−12.

(8) Huntington, J. A. (2009) Slow thrombin is zymogen-like. *J. Thromb. Haemost. 7*, 159−164.

(9) Di Cera, E. (2009) Serine proteases. *IUBMB Life 61*, 510−515.
(10) Kamath, P., Huntington, J. A., and Krishnaswamy, S. (2010) Ligand binding shuttles thrombin along a continuum of zymogen- and proteinase-like states. *J. Biol. Chem. 285*, 28651−28658.
(11) Andreasen, P. A., Egelund, R., and Petersen, H. H. (2000) The plasminogen activation system in tumor growth, invasion, and metastasis. *Cell. Mol. Life Sci. 57*, 25−40.
(12) Danø, K., Behrendt, N., Høyer-Hansen, G., Johnsen, M., Lund, L. R., Ploug, M., and Rømer, J. (2005) Plasminogen activation and cancer. *Thromb. Haemost. 93*, 676−681.
(13) Dupont, D. M., Madsen, J. B., Kristensen, T., Bødker, J. S., Blouse, G. E., Wind, T., and Andreasen, P. A. (2009) Biochemical properties of plasminogen activator inhibitor-1. *Front. Biosci. 14*, 1337−1361.
(14) Lund, I. K., Jögi, A., Rønø, B., Rasch, M. G., Lund, L. R., Almholt, K., Gårdsvoll, H., Behrendt, N., Rømer, J., and Høyer-Hansen, G. (2008) Antibody-mediated targeting of the urokinase-type plasminogen activator proteolytic function neutralizes fibrinolysis in vivo. *J. Biol. Chem. 283*, 32506−32515.
(15) Hosseini, M., Jiang, L., Sørensen, H. P., Jensen, J. K., Christensen, A., Fogh, S., Yuan, C., Andersen, L. M., Huang, M., Andreasen, P. A., and Jensen, K. J. (2011) Elucidation of the contribution of active site and exosite interactions to affinity and specificity of peptidylic serine protease inhibitors using non-natural arginine analogs. *Mol. Pharmacol. 80*, 585−597.
(16) Petersen, L. C., Brender, J., and Suenson, E. (1985) Zymogen-activation kinetics. Modulatory effects of trans-4-(aminomethyl)-cyclohexane-1-carboxylic acid and poly-D-lysine on plasminogen activation. *Biochem. J. 225*, 149−158.
(17) Griffin, J. H. (1995) Blood coagulation. The thrombin paradox. *Nature 378*, 337−338.
(18) Treuheit, N. A., Beach, M. A., and Komives, E. A. (2011) Thermodynamic compensation upon binding to exosite 1 and the active site of thrombin. *Biochemistry 50*, 4590−4596.
(19) Spraggon, G., Phillips, C., Nowak, U. K., Ponting, C. P., Saunders, D., Dobson, C. M., Stuart, D. I., and Jones, E. Y. (1995) The crystal structure of the catalytic domain of human urokinase-type plasminogen activator. *Structure 3*, 681−691.